Design and experimental validation of a piezoelectric actuator tracking control based on fuzzy logic and neural compensation

Cristian Napole *, Oscar Barambones, Mohamed Derbeli, Isidro Calvo

Engineering School of Vitoria, Basque Country University (UPV/EHU), Nieves Cano 12, Vitoria Gasteiz, 01010, Álava, Spain

Abstract

This work proposes two control feedback-feedforward algorithms, based on fuzzy logic in combination with neural networks, aimed at reducing the tracking error and improving the actuation signal of piezoelectric actuators. These are frequently used devices in a wide range of applications due to their high precision in micro- and nanopositioning combined with their mechanical stiffness. Nevertheless, the hysteresis is one the main phenomenon that degrades the performance of these actuators in tracking operations. The proposed control schemes were tested experimentally in a commercial piezoelectric actuator. They were implemented with a dSPACE 1104 device, which was used for signal generation and acquisition purposes. The performance of the proposed control schemes was compared to conventional structures based on proportional-integral-derivative and fuzzy logic in feedback configuration. Experimental results show the advantages of the proposed controllers, since they are capable of reducing the error to significant magnitude orders.

1. Introduction

In the early 1970s, position devices with high-accuracy was constrained to research laboratories but the further improvements in recent years for production and industrial demands provided tangible capabilities for applications [1]. Hence, here is where piezoelectric actuators (PEA) began their expansion in industry, due to their high-precision combined with considerable mechanical stiffness [2]. These are able to produce a mechanical displacement from an electrical excitation, also known as inverse piezoelectric effect [3]. Examples of applications where PEAs take place are for instance in biological cell micro-manipulation which contemplates risky operations like injection where strokes should be around 138 μm [4,5]. Another biological topic is with spinal cord injection robots which have to perforate a ventral horn with an available area of 1 mm^2 [6]. On another different field such as aerospace, PEAs can be used as actuation systems for pneumatic or hydraulic pumps which also may require certain stifness [7]. Other

---

* Corresponding author.
  E-mail address: cristianmario.napole@ehu.eus (C. Napole).

related applications are based on optical focus mechanisms [8], active force generation for vibration absorption [9] and machine tools [10].

Despite the advantages and applications, a piezoelectric material has three known phenomena that can alter its behaviour due to the induced non-linearities. Because a PEA has certain dynamics which correspond to a mass-spring-damper system, undesirable vibrations may happen in a particular operating range (commonly at high input frequencies) [11]. Creep is a dynamical long-term effect that commonly occurs with constant references where the displacement drifts upwards or downwards [12]; this phenomenon, which produces errors that can reach up to 5.5%, is generated as a consequence of a residual polarization which tends to increase (or decrease) in time [13]. Finally, hysteresis reduces the tracking performance, as it can induce errors of around 17% [14].

Hysteresis reduction can be handled from two diverse perspectives: tracking control design or material re-engineering [15]. In regards to the latter mentioned option, according to Park and Shrout, [16] there is a property related to the performance called *piezoelectric coefficient* (also known as d_{33}) which determines the degree of induced strain at a particular electrical field. Thus, a piezoelectric material will display a lower hysteresis but at the expense of decreasing d_{33}, which implies that the material will have less stiffness. Therefore, in this case, we pursed the design of a control strategy.

From the perspective of classic control theory, linear controllers can be a suitable first option for a PEA. The proportional-derivative-integral (PID) scheme has been implemented several times and it is still being employed for comparisons. An interesting study was produced by authors of [17], where they generated a simulated environment with a Bouc-Wen (BW) hysteresis model for the PEA and a PID, tuned by optimisation, was applied. The achieved control parameters were then used in an experimental rig where the outcomes showed a maximum error percentage of around 5%. Another attractive study was presented by Kaci et al. [18], where they developed a strategy of a PID tuned through a linear quadratic regulator for a resonant plate actuated by a PEA. Despite that the aim was unrelated to tracking, authors attained suitable results in terms of vibration control. On the other hand, a similar approach to vibrations rejection with PEAs was carried by Tang et al. [19], where they used Youla parameterization with a PEA to reduce fluctuations of a telescope and results showed an enhanced performance of the system. Nevertheless, hysteresis is a strong nonlinear and undesired effect which limits the operating range with a linear controller [20]. Furthermore, uncertainties like modelling or external loads are commonly present so that linear strategies are limited in this sense due to the actuation bandwidth [21].

Among the diversity of non-linear strategies, sliding mode controllers ones are one of the most frequently used during the last decades due to their robustness [22]. Different combinations were proposed from various authors for several applications where a PEA had an important role. For example, authors of [23] proposed a conventional sliding mode controller (SMC) for tracking control of a micro-gripper. Despite that the control signal was neglected in the analysis, they obtained errors of around 6%. Another example was developed and implemented by Ling et al. [24], where they used a SMC combined with artificial neural networks (ANN); tests were carried with soft curve references in which acceptable errors were accomplished. Differently, an approach akin to robust control was developed by Dong & Tan [25], where they established a composed structure of bounded sub-models; experimental results showed acceptable positioning errors. Other alternatives to SMC were analysed by Zhang et al. [26] where they implemented a robust control compensator based on feedback linearization. Outcomes were gathered from simulation and experiments, where they reached a satisfactory accuracy. Nevertheless, most of the robust strategies mentioned have a major downside in practice related to the chattering; this phenomenon is produced by neglected fast dynamics and with finite sampling rate digital controllers [27].

On the other hand, fuzzy logic control (FLC) is an easy understanding type of structure because it is expressed through linguistic rules that can be tuned according to the knowledge of a particular system [28]. Actually, Sabarianand et al. [29] established that advantages of FLC for PEAs are related to its capability to deal with non-linearities, uncertainties and innacuracy. Also, according to Sobrinho & Junior [30], fuzzy sets have better performance in contrast to conventional techniques in embedded systems. For instance, authors of [31] used a fuzzy logic approach for an atomic force microscope (known to have a bending type PEA) and thus, accuracy is an important objective in this case. The simulation outcomes revealed high accuracy and fast corrections. In terms of force control, Kang et al. [32] implemented a FLC in a commercial PEA where they aimed to reduce the hysteresis and they could achieve a fast convergence a suitable force tracking accuracy. Another interesting study was carried out by authors of [33], where they produced a simulated environment for a nanopositioning platform controlled by a PEA through an integral resonant controller based on FLC; results showed improvements up to 1 μm in contrast with a conventional technique.
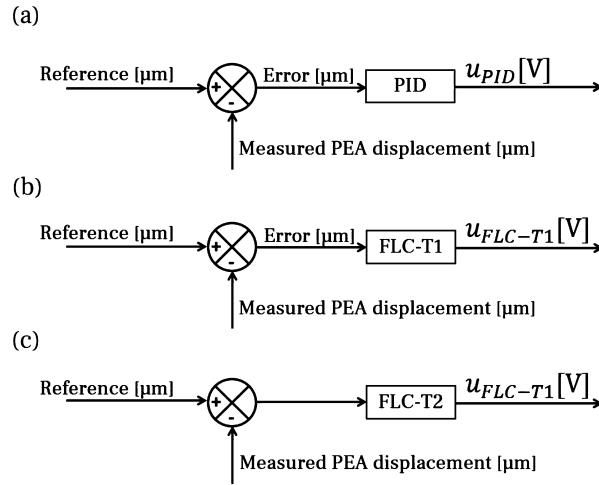
(a)

(b)

(c)

Fig. 1. Conventional control architectures where: (a) is PID, (b) is FLC-T1 and (c) is FLC-T2.

Fuzzy sets that can be described based on classical theoretical techniques are also known as type-1 (FLC-T1) [34]. Nevertheless, there are at least four sources of uncertainties associated to the disadvantages of T1: (1) uncertain linguistic rules, (2) disagreement of expertise, (3) noise associated to activation and (4) measurement data [35]. Hence, this implies that membership functions are not exact as with FLC-T1 because they can be blurred due to these uncertainties [36]. These issues derived the type-2 (FLC-T2) sets which are capable to handle uncertainties and adapt better when definitions are dubious [37]. As a consequence of these augmented capability mirror uncertainties, FLC-T2 is known to have more robustness than FLC-T1 [38]. Also, it has been showed that FLC-T2 is able to perform better than FLC-T1 systems in control related applications [39–42]. In this research, we implemented FLC-T1 and FLC-T2 control structures.

Nevertheless, based on the background research prior to the development of this study, we found that uncompensated feedback controllers have certain issues in PEA tracking control. These are related to the usage limitation of high gain controllers due to low gain margins of feedback controllers and stability performance [29]. Still, a combination of feedback-feedforward structures is recommended since it fuses the individual advantages of each framework to gather a high-performance controller [43]. A feedforward compensation is commonly based on an inverse system model, which implies that model uncertainties can be reduced provided that the feedback controller is well designed in combination with a suitable hysteresis model, as in this case. For this reason, in this investigation, we proposed two novel combinations of feedback-feedforward structures.

Hysteresis models are divided in 2 groups: mathematical and physics based ones. In regards to the latter mentioned, it is used for ferromagnetic hysteresis description due the complex solutions and material dependency [44,45]. On the other hand, mathematical models are divided into operator-based (such as Prandtl-Schlinkskii, Preisach and Kranosel'skii-Pokrovkii [46,47]) and differential equations-based (like Bouc-Wen, Duhem and Backslash [29]). Despite that these models have certain extensions to deal with asymmetric hysteresis, they introduce two major disadvantages: (1) complex numerical solutions which require multi-steps or (2) Runge-Kutta solvers at each time-step and (3) a higher number of parameters (due to the asymmetry, for example) expands the difficulty to achieve a suitable equivalent model [48]. Among the analysed options for feedforward compensation and based on our prior research history [49,50], we found that ANN are characterised by higher precision and easy implementation over mentioned mathematical models [44]. Hence, we conclude that ANN are a suitable option to be implemented in this study for feedforward compensation.

Therefore, the main contributions of this article are as follows:

- At first, the performance of conventional FLC-T1 and FLC-T2 were compared against a PID controller, commonly used for these correlations [51]. Since our goal is to improve the tracking capabilities, we analysed the error and control signals. An schematic structural diagram of these comparisons is provided in Fig. 1.
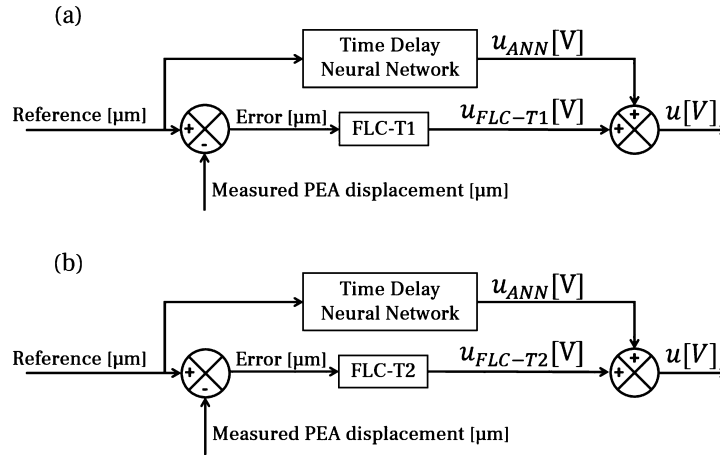
(a)

(b)

Fig. 2. Proposed control architectures where: (a) is FLC-T1 with neural compensation and (b) is the FLC-T2 with neural compensation.

- Secondly, we propose a novel combination of two feedback-feedforward control structures based on FLC-T1 (Fig. 2(a)) and FLC-T2 strategies (Fig. 2(b)), combined with a time delay neural network (TDNN) to control a commercial PEA. These were also analysed in terms of error and control signals.
- In contrast to our prior work were we used FLC in a feedback-feedforward structure [52], we concluded that FLC-T2 was a suitable option to carry with the research and that the employment of ANN could provide better fitting capabilities for the inverse hysteresis model. Additionally, other background related works [53,10], showed the capabilities of FLC-T2 in a feedback structure for PEAS but with an analytical inverse for the feed-forward compensation. Despite that results of these studies showed a suitable performance, we expected to increase the accuracy with the usage of an ANN trained with real data.
- Procedures and results obtained in this report not only can help to improve the accuracy but also the control effort in applications where PEAs have an important role as it was mentioned at the beginning of this section.

We organized the structure of this article as follows. Section 2 provides technical details of the hardware used and description of the commercial PEA hysteresis curve. Section 3 presents explanations about the feedback controllers (PID, FLC-T1 and FLC-T2), the ANN used as feedforward compensator to be combined and the performance metrics that will provide numerical conclusions to be highlighted. Section 4 exposes the experimental results with further discussions of the ANN accuracy, the implementation of the feedback controllers, the combination of the FLC-T1, FLC-T2 with the ANN and a contrast against a modern controller for PEAs proposed in the scientific community [54]. Finally, we summarize the main features of this research in Section 5.

2. Material and methods

2.1. Commercial piezoelectric actuator details

Experiments were based on a real-time platform which was designed for control tuning to set the best performance. The PEA that we used is a Thorlabs PK4FYC2, that is a stack actuator with a linear settlement of piezoelectric layers made of zirconate titanate (PZT) that are attached with epoxy and glass beads. Since the displacement reading needs to be accurate enough, a Wheatstone bridge was included by the manufacturer. The PEA is capable to move in a range of 0-38.5 μm through an input of 0-150 V. The manufacturer reported that the hysteresis can induce a maximum error of 15% in the displacement. For further conciseness, the peripheral hardware link is schematically described in Fig. 3 whereas technical information about these devices is described in our previous study [50]. The real-time experiments were carried out with a sampling frequency of 1 kHz.
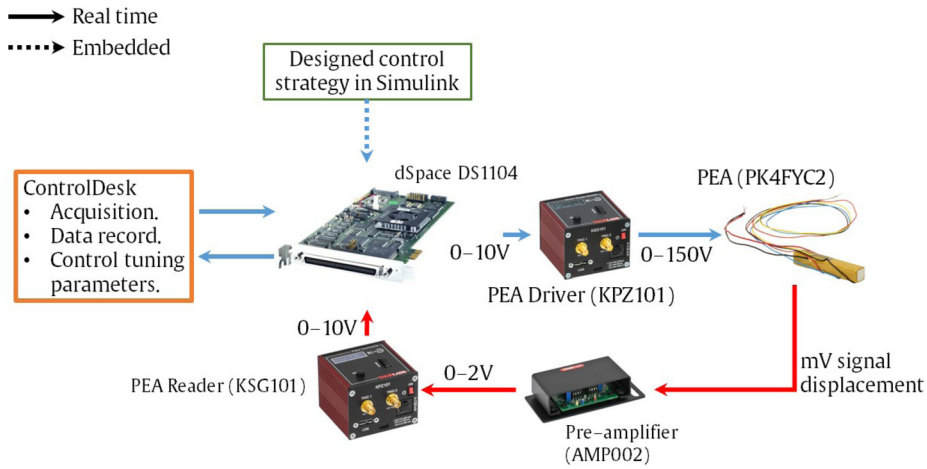
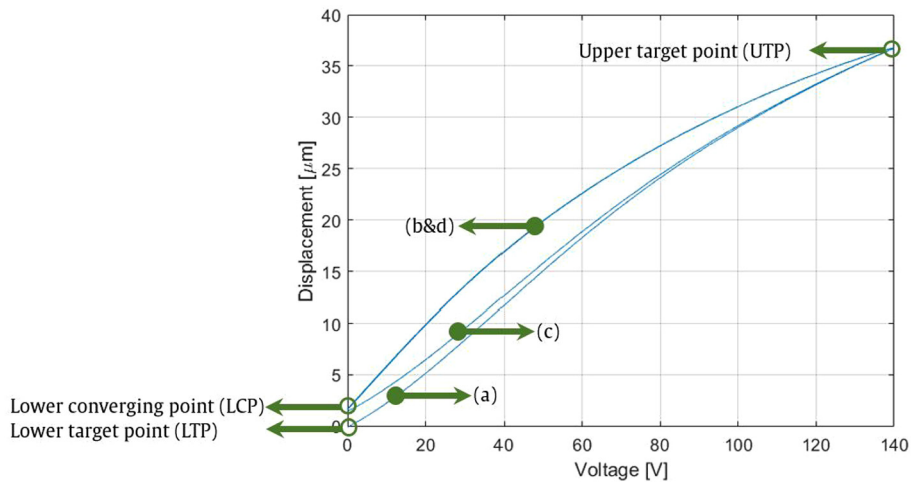Fig. 3. Hardware-software flow configuration used in the experiments.

Fig. 4. Hysteresis of the commercial PEA used in the experiments.

2.2. Hysteresis description and reference generator

A suitable reflection of a hysteresis graph can be reproduced with triangular and senoidal input signals [55]. Nevertheless, triangular waves are preferred to test a high performance system due to their high frequency harmonics, sharp slope change and common usage in PEA applications [56]. Since the hysteresis is usually augmented at high voltages [49], we configured an excitation voltage of 140 V of amplitude and 4 s of period where the outcome is reflected in Fig. 4.

Previously mentioned graph is the output of 2 triangle waves that were recorded from the beginning of the action so that the following description can be performed. At the start, the displacement is null and is echoed in the *lower target point* (LTP); when the voltage starts to increase, the curve *(a)* rises until the *Upper target point* (UTP). Unless that the PEA is re-calibrated to start from a null displacement, *(a)* will only appear once. When the voltage achieves its maximum at the UTP and thus, the PEA reaches also its maximal displacement. The next stage is when the input voltage decreases through curve *(b)* until the *lower converging point* (LCP). If the main features of the input signal are constant along the experiments, the LCP will be a common point for the following curves. Later, the input signal begins to increase again its voltage due to the second period and the curve *(c)* appears and upsurges till the UTP. Following voltage descents is produced along the curve *(d)* that is overlapped with *(b)* and ends in the LCP. Another

important takeaway from previous detailed description, is that the hysteresis of the commercial PEA that we use is asymmetric which increases its complexity at the inverse model design.

In regards to the reference, we developed a linear transformation for tracking. The PEA was driven between 0-150 V, which had to be shifted into a displacement. Based on Fig. 4, a linear equation can be depicted between the LCP and the UTP through Equation (1) where α is the slope among the two mentioned points and p is the vertical gap at the LCP.

$$Displacement[\mu m] = \alpha \cdot Voltage[V] + p \tag{1}$$

3. Design of control schemes

3.1. Performance metrics

We used three metrics for the numerical judgement of the contrast of the proposed algorithms. The first one is the integral of the absolute error (IAE) minimization, a common performance control metric for tuning parameter and optimization that we implemented in the experiments [57,58]. Other metrics used for the analysis were root mean squared error (RMSE) and the relative root mean squared error (RRMSE), also known to be used in tracking performance measurement [59,60,56].

$$\begin{cases} IAE = \sum_{i=1}^{N} |e_i| T_s \\[2em] RMSE = \sqrt{\dfrac{1}{N} \sum_{i=1}^{N} (e_i)^2} \\[2em] RRMSE = \sqrt{\sum_{i=1}^{N} (e_i)^2 / \sum_{i=1}^{N} (r_i)} x\,100 \end{cases} \tag{2}$$

3.2. Time delay neural network

As we explained in the introduction section, PEA hysteresis models have issues to model the dynamics of a real PEA. ANNs is a relatively new tool based on black box concept, which implies that inside structure is unrelated to physical properties of a system [61]. It was found that this could be a suitable tool to achieve compensation voltage for the proposed control structure since it was possible to gather experimental data to develop an inverse model.

According to Ma et al. [62], an ANN is a nonlinear model which is produced from several linear inner connections between neurons with their respective weights and biases. This complex structure has its origins from the nature of brain neurons which have *neuroplasticity*, that is a property of these biological structures to recognize, learn and adjust based on the historical actions [63]. A TDNN has capacity to deal with time series data for identification of dynamical systems [64]. Additionally, in formerly studies it was found that these types of ANNs are able to deal with hysteresis compensation problems [49].

A TDNN resides its structure on three nodes based on an ordinary feed-forward ANN as Fig. 5 shows. The dynamics of the input vector $X(t)$ are gathered through n delayed signals and is then linearly transformed with the weight matrix W_k with the bias vector b_k. Later, it is fed into an activation function such as a *tansig*. The output layer is supplied with the vector $r(t)$ and again linearly changed with the weight matrix W_j and a bias b_j and finally, used as an input in *purelin* activation function.

$$r(t) = tansig\left[\sum_{l=0}^{n} W_j \big(x(t-n)\big) + b_k \right) \right] \tag{3}$$

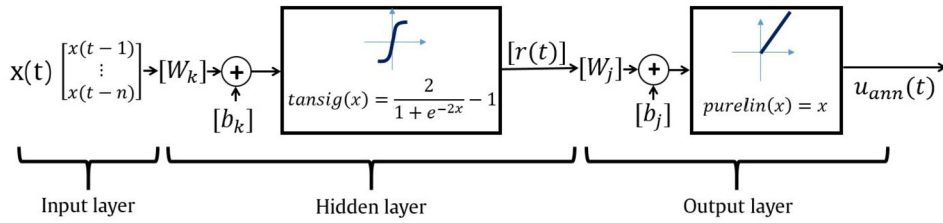$$u_{ann} = purelin\left[W_j \big(r(t)\big) + b_j \right] \tag{4}$$
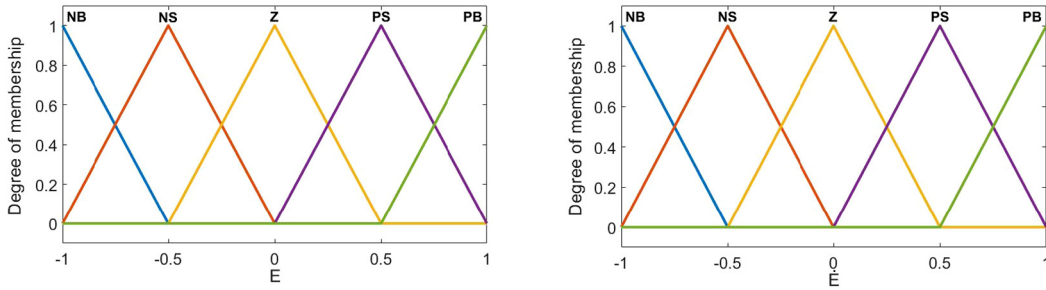
Fig. 5. Time delay neural network structure.

Fig. 6. FLC-T1 Membership functions.

Weights and biases can be defined through a training process gathered from experimental data. In this case, we used MATLAB Deep Learning Toolbox with Bayesian regularization (BR) as it is suggested for data with further noise [65]. Usually, in ANN training, a main cost function used for convergence is the mean-squared error through experimental data which is shown in Equation (5), where P is the number of observations, T_i is the target data and U_i is the ANN output (both at the i-th sample).

$$E_{MSE} = \frac{1}{P} \sum_{i=1}^{P} (T_i - U_i)^2 \tag{5}$$

However, if a training is mainly performed using this cost function, it would resemble in an overfitting. This happens when the ANN fits with the training data but not with the test portion and thus, this would provide an unsuitable overall performance. Thence, BR penalizes the Equation (5) with a different cost functions where the objective is to penalize large weights and aims to generalization. Further technical details can be found in the research made by the authors of [66–68].

3.3. Fuzzy logic control type 1 and 2

FLC is featured by a fuzzifier, base rules, an inference engine and a defuzzifier where, according to [69]: the fuzzifier maps the inputs into the fuzzy set through linguistic variables; an inference engine determines the process in which the fuzzy sets are linked within previous defined base rules (where the designer adds his knowledge about the system), that is commonly done with rules *if-then* [70]; a defuzzifier translates the linguistic rules into numerical values for the output. A FLC-T1 is defined as a set A which is a function based on a universe X into a domain [0, 1], where a membership function of A is defined as μ_A where $0 \leq \mu_A \leq 1$ [71]. Mathematically, this is expressed as follows:

$$A = \left\{ (x, \mu_A(x)) \,|\, x \in X \right\} \tag{6}$$

In this case, we used the error and its derivative as inputs which are scaled through factors like K_e and K_{Ed} into an interval [−1 1]. Later, the fuzzification process is where μ_A membership functions are explicitly defined. In this case, it comprehends triangular overlapped and normalized membership functions as previously mentioned; these are shown in Fig. 6.

Table 1
Linguistic rules.

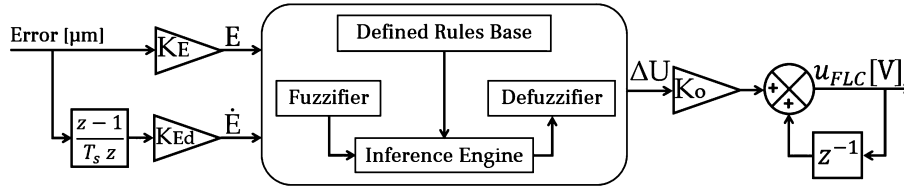| E \ Ė	NB	NS	Z	PS	PB
NB	NB	NM	NM	NS	Z
NS	NM	NM	NS	Z	Z
Z	NM	NS	Z	PS	PM
PS	Z	Z	PS	PM	PM
PB	Z	PS	PM	PM	PB

Fig. 7. Structure of a fuzzy logic controller type-1.

The inference is where previous membership functions are associated with a set of rules in a clear linguistic term such as Equation (7). At this stage, the designer has to employ the knowledge about the system in order to achieve a suitable controller behaviour.

$$R_m : \text{ If } E = B_{1k} \text{ and } \dot{E} = B_{2l} \Rightarrow \Delta U = G_m \tag{7}$$

Therefore, we defined the linguistic rules from Table 1 which were chosen based on the PEA behaviour. When the error is positive and large, a considerable control signal had to be applied to reduce the value. Whenever the error reaches a null value, the control signal required to have a gradual change to avoid unnecessary overshoots. When negative values of error were appreciated, the schedule is symmetrical. We discretized the membership functions in uniform in terms of negative big (NB), negative medium (NM), negative small (NS), zero (Z), positive small (PS), positive medium (PM) and positive big (PB); were we defined these values as -1, -0.66, -0.33, 0, 0.33, 0.66 and 1, respectively. Then, we configured the defuzzification mechanism for the crips outputs in constants that were discretized uniformly in the range of $[-1\ 1]$. Finally, an output gain K_o augments the value of the control signal for a suitable performance.

Previous described type-1 (see Fig. 7) lacks of capabilities to handle uncertainties, therefore Zadeh defined the type-2 sets [72]; this concept was later augmented by Mizomoto and Tanaka [73]. This expansion allows efficacy on a fuzzy set in which uncertainties are difficult to measure or determine. Based on Castillo et al. [74], a fuzzy set of type-2 is usually denoted by $\tilde{A}$ but differently to type-1, there is an upper and lower membership function $\underline{\mu}_{\tilde{A}}(x)$ and $\overline{\mu}_{\tilde{A}}(x)$. This is defined in Equation (8). These limits are associated with a type-2 feature known as *footprint of uncertainty* (FOU), that is defined in Equation (9). In other words, the FOU expresses uncertainty in the definition of type-2 sets membership functions [75–77]; thus, this is an advantage over type-1 sets which require exact values in their membership function definition. For our case, the FOU is graphically expressed in Fig. 9.

$$\tilde{A} = \left\{ \left((x, u), 1 \right) \middle| \forall x \in X, \forall u \in J_x \subseteq [0, 1] \right\} \tag{8}$$

$$FOU(\tilde{A}) = \left\{ (x, u) \middle| x \in X \text{ and } u \in \left[\underline{\mu}_{\tilde{A}}(x), \overline{\mu}_{\tilde{A}}(x) \right] \right\} \tag{9}$$

The mechanism of fuzzification of fuzzy sets type-2 is analogue to type-1, although the linguistic form of the inference is defined based on the uncertainties linked to the main feature. Therefore, the rules are expressed in the form of Equation (10). Since the FLC-T2 has a range of uncertainties, the defuzzification process has an extension known as the *type-reduction*, which implies the calculation of a centroid. In this case, we used the Karnik-Mendel which is a common used method in fuzzy sets type-2 where the goal is to seek for crucial points that combine the upper and lower membership function limits [78]; further features about this tool can be found in the study of the authors [79]. A schematic resume of the described technique is shown in Fig. 8.
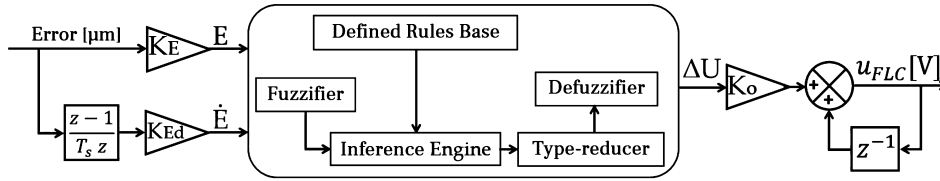
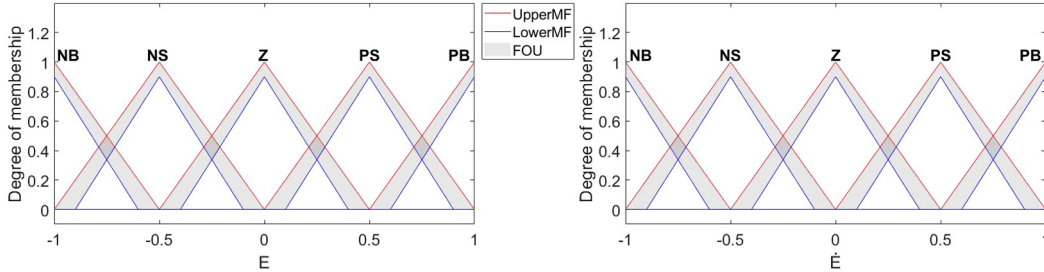Fig. 8. Structure of a fuzzy logic controller type-2.

Fig. 9. FLC-T2 Membership functions.

$$R_m : \text{ If } E = \tilde{B}_{1k} \text{ and } \dot{E} = \tilde{B}_{2l} \Rightarrow \Delta U = \tilde{G}_m \tag{10}$$

3.4. Proportional-derivative-integral controller

PID controllers had been design and implemented in vast applications due to their simple structure to provide satisfactory results. In this case, it was used the discrete PID controller from MATLAB/Simulink Control System Toolbox and the expression is the one provided in Equation (11) where T_s, K_p, K_i and K_d are, respectively, the sampling time, proportional, integral and derivative gains [80]. Additionally, it was included a derivative filter to limit the high frequency gain which parameter is N [81]. Due to the available capabilities provided by Simulink, a conditional integration antiwind-up strategy was configured as well [82]. Even-though that these parameters can be tuned with Ziegler-Nichols, Cohen-Coon, frequency response, relay feedback and critical ratio methods, these induce difficulties to gather the optimal parameters in variable system conditions [83,84]. Instead we used the minimization of IAE which was formerly explained.

$$K_p + K_i T_s \frac{1}{z-1} + K_d \frac{N}{1 + N T_s \frac{1}{z-1}} \tag{11}$$

4. Results and discussion

4.1. Neural network verification

We trained the ANN with recorded data from experiments were we settled a triangular signal input of 140 V with a period of 4 s and 1 kHz of sampling frequency. Nevertheless, during the ANN configuration, this was reversed to produce the inverse model so that the output is a compensation voltage. The 70% of the total acquired data was used for training, 15% for evaluation and the rest was used in testing. As we previously explained, we used a BR for training and implemented through MATLAB in a Dell Precision3640 configured with 7 cores. The training lasted for 16.5 hours with 3927 iterations.

The outcomes are presented in the Fig. 10 where a 4 s cycle is contrasted with a hysteresis fitting with its approximation error. The first rise that is performed between 0 and 2 s, where the error has fluctuations which are between ± 0.2 V. In the first slope change (at 2 s), a sharp and expected change appears where the error value switches from 0.25 V to -0.25 V. Along the voltage descent (last 2 s), the error has a negative value in most of the range although it did not exceed -0.2 V. Also, for this case, we calculated the RMSE which is equal to 0.0964 V and it provides a reasonable accuracy that can be enhanced with feedback controllers.
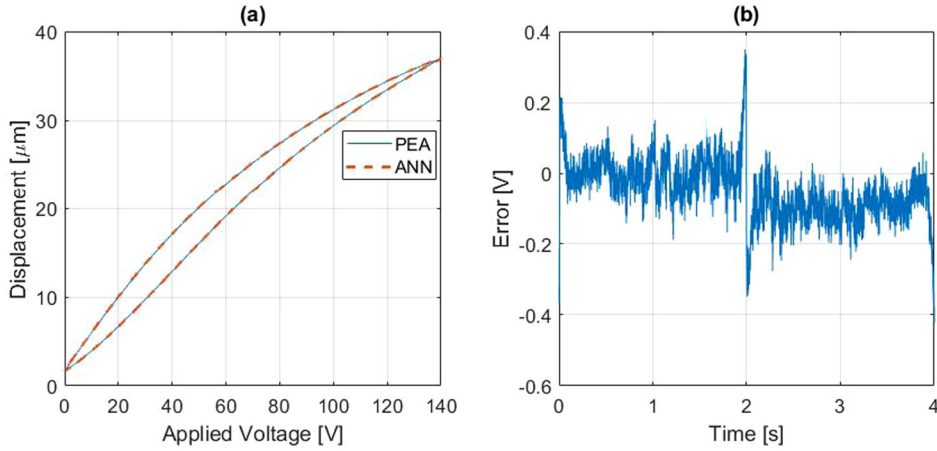
Fig. 10. ANN capability to fit with the PEA studied nonlinearity where: (a) is the hysteresis graph and (b) is the fitting error.
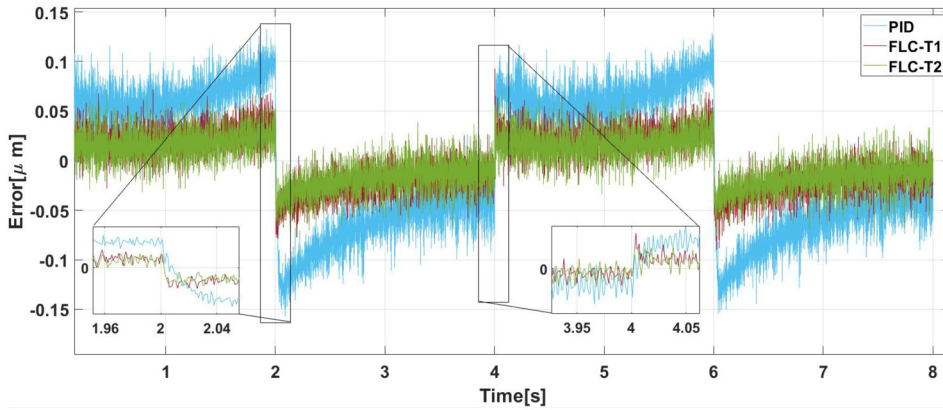

Fig. 11. Error acquired during the test of the feedback controllers.

4.2. Experimental comparison of feedback controllers

Feedback control structures such as PID, FLC-T1 and FLC-T2 were implemented in the dSPACE 1104 platform. We recorded the error and the control signal which were overlapped for a suitable contrasted comparison. We tuned the control parameters in real time through the IAE minimization. Additionally, we took into account the limits of the actuator, so we included saturations limits to avoid damaging the hardware. PID controller gains were established as 10, 1000, 0.001 and 100, respectively, for the K_p, K_i, K_d and N. On the other hand, the FLC-T1 reached an acceptable performance with K_e, Kd and K_b as 12, 0.0006 and 0.58, respectively. FLC-T2 achieved a suitable behaviour with K_e, Kd and K_b, respectively, as 21, 0.0002 and 0.14. The FOU was established as 10% and further details of this are explained in following section.

The first experiment outcomes are provided in Fig. 11 to analyse the error. In this case, we will show 2 cycles (or 8 s) in order to interpret the full range behaviour. Therefore, in the first rise (before 2 s), the three controllers show a similar behaviour at different amplitudes. For instance, both FLC types have a lower value than the PID but the curvature trend tends to be similar. Nevertheless, this increases differently after the first second in both FLC controllers and even the FLC-T2 tends to have a better performance that the others since the amplitude lowers its value.

One of the first critical point is at 2 s which is were the displacement reaches the UTP and the slope changes its sign. At this moment, the error of the three controllers also changed its sign suddenly due to the sharp variation. Whereas the PID acts with a lower compensation, both FLC have a faster correction in contrast. Also, the FLC-T2 and FLC-T1 performed similarly in the zoomed window in terms of amplitude and time response.

Table 2
Metrics comparison for feedback controllers.

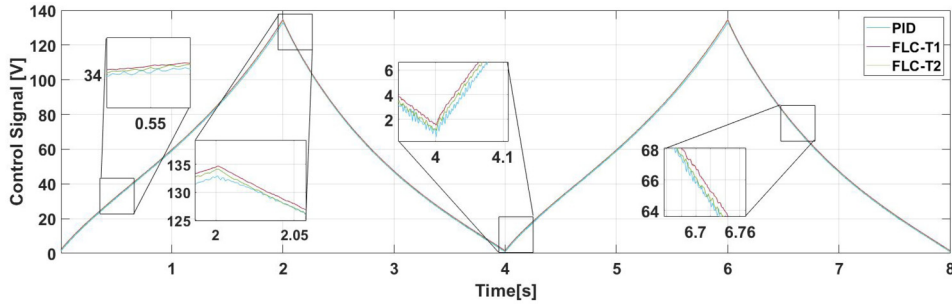| Controller	IAE		RMSE		RRMSE
	Value	Diff. [%]	Value [μm]	Diff. [%]	Value [%]
PID	0.5242	-	0.0706	-	0.3367
FLC-T1	0.1912	63.52	0.0278	60.62	0.1327
FLC-T2	0.1672	68.08	0.0252	64.3	0.1201

Fig. 12. Control signal acquired during the test of the feedback controllers.

After the first slope change, the reference descents where the error tends to show a reciprocated situation, like in the rise. However, the PID corrected with a higher amplitude difference in comparison to both types of FLC, which again have a similar demeanour. The PID has a curved correction which lasts 1.5 s until it can reach levels of the FLC, that is near 3.5 s. Moreover, the PID error compensation has higher amplitude values in contrast to the FLC-T1 and FLC T-2 due to the peaks that can be shown near 2.7 s and 3.2 s.

Finally at the LCP, the circumstance was fairly different to the one from 2 s since the controllers behaved more similar. Nonetheless, the PID still reacted worse in terms of amplitude but the correction in time seemed to be faster, specially after 4 s where the settling time was faster than before (at 2 s). Additionally, the FLC-T2 tended to act better than FLC-T1 after the change; the amplitude was slight lower where certain peaks averaged the null value.

A further precision analysis was carried with the performance metrics that we calculated in Table 2. We referred all the values to the PID controller as it showed the lowest effectiveness. The IAE achieved by the PID exhibited 0.5242, which was enhanced by the FLC-T1 with 63.52% and even further by the FLC-T2 with 68.08% of difference. Additionally, this discrepancy it is also shown in the RMSE with a modest 4% extra for the FLC-T2. Finally, the RRMSE displays that the both FLC types had near 3 times higher accuracy than the PID.

In regards to the control signal, Fig. 12 displays the generated signal of each control framework implemented in a feedback mode. As a first appreciation, it can be seen that there is a lack of saturations which can damage the actuator. Nevertheless, there are certain oscillations which deserve an in-depth analysis: in most of the zoomed windows, we can see quick variations which belong to the PID controller specially in the range of the LCP (around 4 s) and in the descent (near 6.7 s). This is an important feature to highlight since it not only can lead to an actuator wear but also to extra energy consumption. Nevertheless, FLC-T1 and FLC-T2 behaved similarly in the last mentioned points of interests but with a slight better performance for the FLC-T2 in the rising as it can be seen near 0.5 s at the uprising.

4.3. Experimental comparison of feedback controllers with neural compensation

After the analysis of feedback structures, we implemented and acquired the outcomes of the advanced proposed controllers. In this case, in order to enhance the proposed algorithms, we made a sweep FOU values in which we could observe a candidate percentage depending on the minimal IAE achieved. This is resumed in Table 3 were the values of IAE were calculated in 40 s of experiment. It can be seen that 10% unveiled the minimum IAE, which we chose for the experiments.

In terms of error tracking, the first feature seen in Fig. 13 is the magnitude order change in the vertical axis which unquestionably lowered its value in contrast to previous analysis. Where former examination showed a curved

Table 3
Variation of FOU percentage and the IAE
achieved in each case.

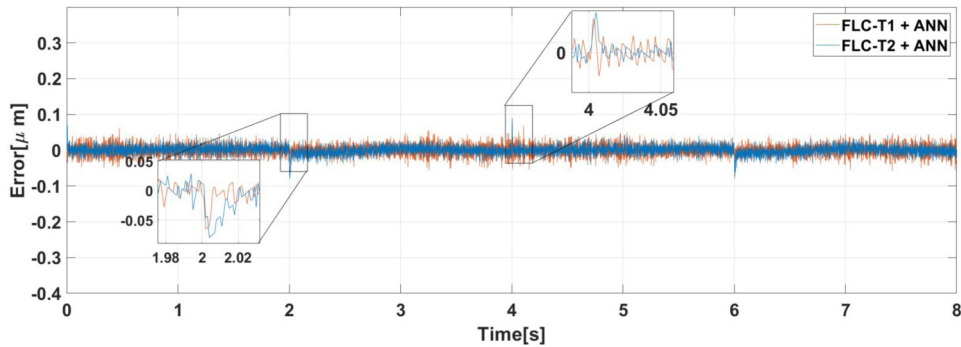| FOU Percentage [%]	IAE Value
5	0.3852
10	0.3850
15	0.3863
20	0.3901
30	0.3896
50	0.3922

Fig. 13. Error acquired during the test of the feedback-feedforward controllers.

Table 4
Metrics comparison for feedback-feedforward controllers.

Controller	IAE		RMSE		RRMSE
	Value	Diff. [%]	Value [μm]	Diff. [%]	Value [%]
FLC-T1-ANN	0.1039	-	0.0164	-	0.078
FLC-T2-ANN	0.0807	22.32	0.0129	21.34	0.061

variation that changed its sign every 1 s, the current displays a constant variation with less than 0.1 μm that oscillates around the null value. Based on previous subsection, we highlighted the slope changes which are the main critical points.

At the first slope sign shift at 2 s, both controllers behaved similarly although the FLC-T1-ANN, seems to have a slightly faster correction. Oppositely, when the slope switches from negative to positive at 4 s, the situation has a modest change where the FLC-T2-ANN compensates the error. On the other sides, it can be seen that the FLC-T2-ANN has a suitable performance due to the error amplitude which lower than the alternative option.

In regards to the metrics, Table 4 displays the metrics calculated for the advanced controllers. Although the magnitudes are similar, FLC-T1-ANN showed the lower values in overall and thus it was used as a reference for the percentage calculation. The FLC-T2-ANN achieved better outcomes since the difference is 21.32% and 21.34% for the IAE and the RMSE, respectively. On the other hand, the RRMSE shows a meager difference, which is favourable for the FLC-T2-ANN.

Finally, the control signal of these proposed architectures is shown in Fig. 14. In the previous study, saturations or sharp changes are unseen but certain points deserve to be highlighted. During the rise in the first 2 s, both controllers have a similar demeanour which can also be seen during the first change at the UTP. Also, a similar situation is seeing during the descent that is pointed near 6.7 s. Nevertheless, at the LTP, the FLC-T2-ANN shows a disadvantage because its signal contains further variations in contrast to the alternative.
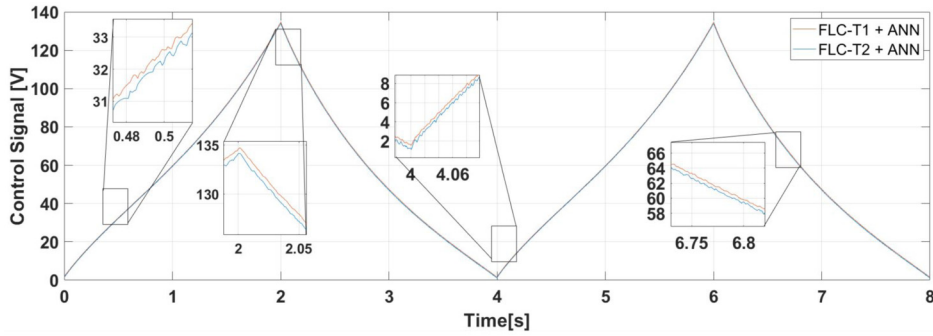
Fig. 14. Control signal acquired during the test of the feedback-feedforward controllers.

Table 5
Obtained mechanical and hysteresis model parameters from experimental data.

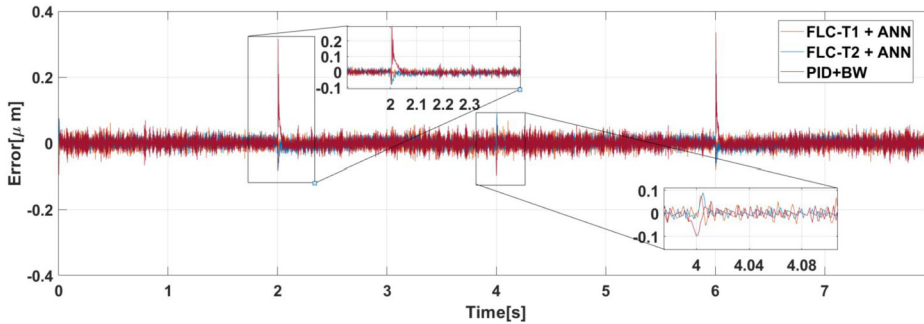|	Values	Units
Mass (m)	0.431	kg
Damping (d)	1340	N·s/m
Stiffness (k)	0.3863	N/m
piezoelectric coefficient (d)	$2.56 \cdot 10^{-7}$	m/V
α	0.5048	-
β	0.0931	-
γ	0.0052	-

Fig. 15. Error signal acquired during the test of a PID-BW hysteresis model and contrasted with previously proposed feedback-feedforward controllers.

4.4. Experimental comparison of fuzzy logic controllers with neural compensation against a modern approach

In order to show the contribution of the designed advanced controllers, we selected a modern approach which was then implemented at the experimental platform. Recently, Zhou et al. [54] developed a tracking strategy for PEAs with further potential applications in aeronautical industry. The controller was designed based on a PID joined with a feedforward compensation related to a Bouc-Wen model. The constants from the PID were the same as previously achieved (showed in Section 4.2) through minimization of IAE.

The values related to the Bouc-Wen model were obtained with the same experimental data that was used for the ANN training. Further explanations of the model and parameter descriptions can be found in the work of Son et al. [85]. We used Parameter Estimator Toolbox from Simulink and configured it with nonlinear least squared and Trust-Region-Reflective algorithm. The obtained parameters are outlined in the following Table 5.

The first characteristic that we contrast was the error tracking that is overlapped with FLC-T1-ANN and FLC-T2-ANN previous results and shown in Fig. 15. Even-though the PID-BW develops a suitable behaviour along the experiment, remarkable features were meant to be analysed. These are coincident with the reference slope changes at

Table 6
Metrics comparison for PID-BW with feedback-feedforward controllers.

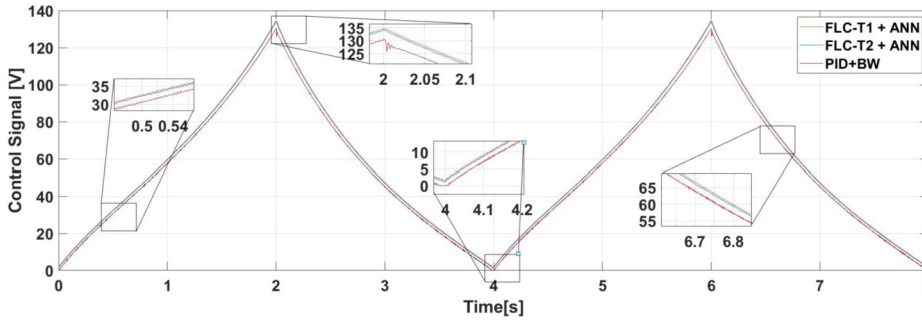| Controller	IAE		RMSE		RRMSE
	Value	Diff. [%]	Value [μm]	Diff. [%]	Value [%]
PID-BW	0.1187	-	0.0202	-	0.096
FLC-T1-ANN	0.1039	12.46	0.0164	18.81	0.078
FLC-T2-ANN	0.0807	32.01	0.0129	36.13	0.061

Fig. 16. Control signal acquired during the test of a PID-BW hysteresis model and contrasted with previously proposed feedback-feedforward controllers.

2 s and 4 s (then periodically repeated). The first slope change at 2 s, which is pointed in the first zoomed window, shows the PID-BW is unable to correct with a fast response as the other neural fuzzy controllers. Moreover, the value of error is much higher at the peak which can be seen by the vertical axis, which value reaches around 0.2 μm. At the downstream of 4 s, it can be seen the inverse slope change. Despite that the absolute values of the error are similar, the PID-BW counterbalances the error slower than the other controllers.

As previously done, the numerical metrics were also calculated and mirrored in Table 6. In this case, the percentages were referred to the PID-BW. We observed relevant differences in the IAE values where the PID-BW gathered the higher ones. Hence, the percentage difference showed the FLC-T2-ANN had the best relative performance as it developed around 32% and the FLC-T1-ANN 12.46%. Similar values are shown as well in the RMSE where again, the FLC-T2-ANN had the best demeanour. As it was expected, the values of RRMSE exhibit the same performance.

We also acquired the control signal from the PID-BW, contrasted in Fig. 16. Relevant points to be analysed are exposed in the zoomed windows. During constant slope following at climbing and descending, it can be seen that the PID-BW generated higher chattering than adversaries controllers. On the other hand, the slope changes at 2 and 4 seconds developed important facts to be considered. After the first shift, PID-BW generated a significant transient response which lasted during few steps. Seconds later, at 4 s, the PID-BW saturates the control signal at 0 V during some steps.

5. Conclusions

In this article, it was shown that hysteresis is one of the main phenomena that degrades the performance of PEAs in tracking operations. Thus, we analysed the applicability of different feedback-feedforward control structures based on fuzzy logic control strategies, known as FLC-T1 and FLC-T2. We reviewed that the advantage of using FLC-T2 over FLC-T1 is the resolution of the uncertainties by means of the membership functions. These controllers were connected to a trained TDNN in a feedback-feedforward structure which was expected to increase the accuracy of FLC-T1 and FLC-T2 in a feedback configuration. Therefore, the strategies were: (1) PID, (2) FLC-T1, (3) FLC-T2, (4) FLC-T1-ANN and (5) FLC-T2-ANN.

The five control schemes were embedded in an experimental test rig which involved a real PEA. The experimental setup included: a commercial PEA and its peripheral hardware (both provided by Thorlabs) and a dSPACE 1104 platform, which was used for signal generation and acquisition purposes. A triangular signal was chosen as reference, since this is a complex curve to be followed due to the sharp changes and harmonics.

Experiments were carried out with FLC-T1, FLC-T2 and PID control schemes. The latter is a was chosen because is a common approach used for tracking control operations of PEAs. Thus, results showed the superiority of the FLC controllers against PID algorithm in the accuracy and control signal. Actually, the fuzzy schemes displayed an improvement over the PID of around 60% at tracking operations.

Additionally, FLC-T1 and FLC-T2 were combined in a feedback-feedforward structure with the TDNN. Experimental results exhibit an evident accuracy enhancement which was reflected in the magnitude order of the error. Nevertheless, FLC-T2-ANN unveils the best performance due to its capability to cope with the uncertainties. This was observed in the graph and numerical error analysis which coexisted with a suitable control signal.

Additionally, FLC-T1-ANN and FLC-T2-ANN were compared against a modern control approach gathered from the scientific community. This controller was a PID with a hysteresis compensation model made with Bouc-Wen theory. Experiments were carried with this strategy. Results in graphs and numerical metrics showed better performance for the proposed fuzzy neural strategies.

The presented analysis, based on FLC-T2 and FLC-T1 joined with ANN, provided several benefits over conventional algorithms like PID or their feedback structure without the neural compensation. These control schemes achieved considerable improvements in terms of accuracy, paving the way to high precision applications. In addition, suitable control signals were generated aimed at reducing the efforts at the PEAs.

Declaration of competing interest

The authors declare that they have no known competing financial interests or personal relationships that could have appeared to influence the work reported in this paper.

Data availability

No data was used for the research described in the article.

Acknowledgements

References

[1] S. Arnold, P. Pertsch, K. Spanner, Piezoelectric Positioning, Springer Berlin Heidelberg, Berlin, Heidelberg, 2008, pp. 279–297, Ch. 12.

[2] F. Chen, Y. Gao, W. Dong, Z. Du, Design and control of a passive compliant piezo-actuated micro-gripper with hybrid flexure hinges, IEEE Trans. Ind. Electron. 68 (11) (2021) 11168–11177, https://doi.org/10.1109/TIE.2020.3032921.

[3] M. Santhya, A. Upadhya, K. Navin, S. Kulkarni, M. Rao, Recent trends in piezoelectric actuators for precision motion and their applications: a review, Smart Mater. Struct. 30 (2020) 013002, https://doi.org/10.1088/1361-665X/abc6b9.

[4] P. Wang, Q. Xu, Design and testing of a flexure-based constant-force stage for biological cell micromanipulation, IEEE Trans. Autom. Sci. Eng. 15 (3) (2018) 1114–1126, https://doi.org/10.1109/TASE.2017.2733553.

[5] Y. Hu, J. Ma, Y. Zhang, J. Li, Y. Hu, J. Wen, Performance comparison of two motion modes of a piezoelectric inertial linear motor and its potential application in cell manipulation, Mech. Syst. Signal Process. 157 (2021) 107743, https://doi.org/10.1016/j.ymssp.2021.107743.

[6] W. Meinhold, D.E. Martinez, J. Oshinski, A.-P. Hu, J. Ueda, A direct drive parallel plane piezoelectric needle positioning robot for MRI guided intraspinal injection, IEEE Trans. Biomed. Eng. 68 (3) (2021) 807–814, https://doi.org/10.1109/TBME.2020.3020926.

[7] T.V.K. Vo, T.M. Lubecki, W.T. Chow, A. Gupta, K.H.H. Li, Large-scale piezoelectric-based systems for more electric aircraft applications, Micromachines 12 (2) (2021), https://doi.org/10.3390/mi12020140.

[8] Q. Chang, Y. Liu, J. Deng, S. Zhang, W. Chen, Design of a precise linear-rotary positioning stage for optical focusing based on the stick-slip mechanism, Mech. Syst. Signal Process. 165 (2022) 108398, https://doi.org/10.1016/j.ymssp.2021.108398.

[9] S. Mohanty, S. Dwivedy, Linear and nonlinear analysis of traditional and non-traditional piezoelectric vibration absorber with time delay feedback for simultaneous resonance conditions, Mech. Syst. Signal Process. 161 (2021) 107980, https://doi.org/10.1016/j.ymssp.2021.107980.

[10] D. Li, H. Cao, X. Chen, Fuzzy control of milling chatter with piezoelectric actuators embedded to the tool Holder, Mech. Syst. Signal Process. 148 (2021) 107190, https://doi.org/10.1016/j.ymssp.2020.107190.

[11] G.M. Clayton, S. Tien, A.J. Fleming, S.O.R. Moheimani, S. Devasia, Hysteresis and vibration compensation in piezoelectric actuators by integrating charge control and inverse feedforward, in: 4th IFAC Symposium on Mechatronic Systems, IFAC Proc. Vol. 39 (16) (2006) 812–818, https://doi.org/10.3182/20060912-3-DE-2911.00140.

[12] M.S. Rana, H.R. Pota, I.R. Petersen, A survey of methods used to control piezoelectric tube scanners in high-speed AFM imaging, Asian J. Control 20 (4) (2018) 1379–1399, https://doi.org/10.1002/asjc.1728.

[13] K.K. Leang, A.J. Fleming, Tracking Control for Nanopositioning Systems, Springer International Publishing, Cham, 2016, pp. 213–244, Ch. 7.

[14] R. Changhai, S. Lining, Hysteresis and creep compensation for piezoelectric actuator in open-loop operation, Sens. Actuators A, Phys. 122 (1) (2005) 124–130, https://doi.org/10.1016/j.sna.2005.03.056, sSSAMW 04.

[15] D. Damjanovic, Hysteresis in Piezoelectric and Ferroelectric Materials, vol. 3, Elsevier, 2006, pp. 337–465, Ch. 4.

[16] S.-E. Park, T.R. Shrout, Ultrahigh strain and piezoelectric behavior in relaxor based ferroelectric single crystals, J. Appl. Phys. 82 (4) (1997) 1804–1811, https://doi.org/10.1063/1.365983.

[17] B. Ding, Y. Li, X. Xiao, Y. Tang, Optimized PID tracking control for piezoelectric actuators based on the Bouc-Wen model, in: 2016 IEEE International Conference on Robotics and Biomimetics (ROBIO), 2016, pp. 1576–1581.

[18] A. Kaci, C. Giraud-Audine, F. Giraud, M. Amberg, B. Lemaire-Semail, LQR based MIMO-PID controller for the vector control of an under-damped harmonic oscillator, Mech. Syst. Signal Process. 134 (2019) 106314, https://doi.org/10.1016/j.ymssp.2019.106314.

[19] T. Tang, S. Xu Niu, T. Yang, B. Qi, Q. Liang Bao, Vibration rejection of tip-tilt mirror using improved repetitive control, Mech. Syst. Signal Process. 116 (2019) 432–442, https://doi.org/10.1016/j.ymssp.2018.06.060.

[20] Z. Chi, Recent advances in the control of piezoelectric actuators, Int. J. Adv. Robot. Syst. 11 (2014), https://doi.org/10.5772/59099.

[21] W. Oates, R. Smith, Nonlinear optimal tracking control of a piezoelectric nanopositioning stage, in: Proceedings of SPIE - the International Society for Optical Engineering, vol. 6166, 2006.

[22] Y. Hu, H. Wang, Robust tracking control for vehicle electronic throttle using adaptive dynamic sliding mode and extended state observer, Mech. Syst. Signal Process. 135 (2020) 106375, https://doi.org/10.1016/j.ymssp.2019.106375.

[23] J. Zhang, Y. Yang, J. Lou, Y. Wei, L. Fu, Development and hybrid position/force control of a dual-drive macro-fiber-composite microgripper, Sensors 18 (4) (2018), https://doi.org/10.3390/s18041301.

[24] J. Ling, Z. Feng, D. Zheng, J. Yang, H. Yu, X. Xiao, Robust adaptive motion tracking of piezoelectric actuated stages using online neural-network-based sliding mode control, Mech. Syst. Signal Process. 150 (2021) 107235, https://doi.org/10.1016/j.ymssp.2020.107235.

[25] R. Dong, Y. Tan, Nonlinear robust control of positioning stage using piezoelectric actuator, in: 2018 IEEE 8th Annual International Conference on CYBER Technology in Automation, Control, and Intelligent Systems (CYBER), 2018, pp. 204–207.

[26] Y. Chen, M. Huang, Y. Tsai, Nonlinear control design of piezoelectric actuators with micro positioning capability, Microsyst. Technol. (2019), https://doi.org/10.1007/s00542-019-04437-9.

[27] V. Utkin, H. Lee, Chattering problem in sliding mode control systems, in: 2nd IFAC Conference on Analysis and Design of Hybrid Systems, IFAC Proc. Vol. 39 (5) (2006) 1, https://doi.org/10.3182/20060607-3-IT-3902.00003.

[28] M. Chandrashekhar, R. Ganguli, Uncertainty handling in structural damage detection using fuzzy logic and probabilistic simulation, Mech. Syst. Signal Process. 23 (2) (2009) 384–404, https://doi.org/10.1016/j.ymssp.2008.03.013.

[29] D.V. Sabarianand, P. Karthikeyan, T. Muthuramalingam, A review on control strategies for compensation of hysteresis and creep on piezo-electric actuators based micro systems, Mech. Syst. Signal Process. 140 (2020), https://doi.org/10.1016/j.ymssp.2020.106634.

[30] A.S.F. Sobrinho, F.G. Junior, Type-1 fuzzy logic algorithm for low cost embedded systems, Comput. Electr. Eng. 88 (2020) 106861, https://doi.org/10.1016/j.compeleceng.2020.106861.

[31] M. Korayem, H. Khaksar, A. Mousavi, Modeling and control of probe distance, substrate and probe of AFM using AFSMC in the presence of disturbances, Mech. Syst. Signal Process. 152 (2021) 107458, https://doi.org/10.1016/j.ymssp.2020.107458.

[32] S. Kang, H. Wu, X. Yang, Y. Li, Y. Wang, Model-free robust finite-time force tracking control for piezoelectric actuators using time-delay estimation with adaptive fuzzy compensator, Trans. Inst. Meas. Control 42 (3) (2020) 351–364, https://doi.org/10.1177/0142331219869708.

[33] M. Altaher, S.S. Aphale, Fuzzy-enhanced dual-loop control strategy for precise nanopositioning, in: 2017 International Symposium on Computer Science and Intelligent Controls (ISCSIC), 2017, pp. 73–81.

[34] J.M. Mendel, Introduction, Springer International Publishing, 2017, pp. 1–23, Ch. 1.

[35] J. Mendel, R. John, Type-2 fuzzy sets made simple, IEEE Trans. Fuzzy Syst. 10 (2) (2002) 117–127, https://doi.org/10.1109/91.995115.

[36] J.M. Mendel, Sources of Uncertainty, Springer International Publishing, Cham, 2017, pp. 245–258, Ch. 6.

[37] D. Wu, On the fundamental differences between interval type-2 and type-1 fuzzy logic controllers, IEEE Trans. Fuzzy Syst. 20 (5) (2012) 832–848, https://doi.org/10.1109/TFUZZ.2012.2186818.

[38] P.J. Gaidhane, M.J. Nigam, A. Kumar, P.M. Pradhan, Design of interval type-2 fuzzy precompensated PID controller applied to two-DOF robotic manipulator with variable payload, ISA Trans. 89 (2019) 169–185, https://doi.org/10.1016/j.isatra.2018.12.030.

[39] J. Huang, M. Ri, D. Wu, S. Ri, Interval type-2 fuzzy logic modeling and control of a mobile two-wheeled inverted pendulum, IEEE Trans. Fuzzy Syst. 26 (4) (2018) 2030–2038, https://doi.org/10.1109/TFUZZ.2017.2760283.

[40] K.A. Naik, C.P. Gupta, Performance comparison of type-1 and type-2 fuzzy logic systems, in: 2017 4th International Conference on Signal Processing, Computing and Control (ISPCC), 2017, pp. 72–76.

[41] C.-A. Bojan-Dragos, R.-E. Precup, S. Preitl, R.-C. Roman, E.-L. Hedrea, A.-I. Szedlak-Stinean, GWO-based optimal tuning of type-1 and type-2 fuzzy controllers for electromagnetic actuated clutch systems, IFAC-PapersOnLine 54 (4) (2021) 189–194, https://doi.org/10.1016/j.ifacol.2021.10.032.

[42] J.R. Nayak, B. Shaw, B.K. Sahu, Application of adaptive-SOS (ASOS) algorithm based interval type-2 fuzzy-PID controller with derivative filter for automatic generation control of an interconnected power system, Eng. Sci. Technol. Int. J. 21 (3) (2018) 465–485, https://doi.org/10.1016/j.jestch.2018.03.010.

[43] J. Peng, X. Chen, A survey of modeling and control of piezoelectric actuators, Mod. Mech. Eng. 03 (2013) 1–20, https://doi.org/10.4236/mme.2013.31001.

[44] M. Armin, P. Roy, S. Das, A survey on modelling and compensation for hysteresis in high speed nanopositioning of AFMs: observation and future recommendation, Int. J. Autom. Comput. 17 (2020), https://doi.org/10.1007/s11633-020-1225-4.

[45] G. Xue, P. Zhang, Z. He, D. Li, Z. Yang, Z. Zhao, Modification and numerical method for the Jiles-Atherton hysteresis model, Commun. Comput. Phys. 21 (3) (2017) 763–781, https://doi.org/10.4208/cicp.050615.300816a.

[46] M. Al Janaideh, O. Aljanaideh, Further results on open-loop compensation of rate-dependent hysteresis in a magnetostrictive actuator with the Prandtl-Ishlinskii model, Mech. Syst. Signal Process. 104 (2018) 835–850, https://doi.org/10.1016/j.ymssp.2017.09.004.

[47] J. Fang, J. Zhao, L. Zhang, C. Li, W. Zhong, L. Zhang, Fuzzy sliding mode control of piezo-driven stage, Rev. Sci. Instrum. 93 (1) (2022) 015011, https://doi.org/10.1063/5.0075029.

[48] N. Vaiana, S. Sessa, L. Rosati, A generalized class of uniaxial rate-independent models for simulating asymmetric mechanical hysteresis phenomena, Mech. Syst. Signal Process. 146 (2021) 106984, https://doi.org/10.1016/j.ymssp.2020.106984.

[49] C. Napole, O. Barambones, I. Calvo, J. Velasco, Feedforward compensation analysis of piezoelectric actuators using artificial neural networks with conventional PID controller and single-neuron PID based on Hebb learning rules, Energies 13 (15) (2020), https://doi.org/10.3390/en13153929.

[50] C. Napole, O. Barambones, M. Derbeli, I. Calvo, Advanced trajectory control for piezoelectric actuators based on robust control combined with artificial neural networks, Appl. Sci. 11 (16) (2021), https://doi.org/10.3390/app11167390.

[51] J. Mendel, Type-1 Fuzzy Systems: Design Methods and Applications, Springer International Publishing, 2017, pp. 161–244, Ch. 4.

[52] C. Napole, O. Barambones, I. Calvo, M. Derbeli, M.Y. Silaa, J. Velasco, Advances in tracking control for piezoelectric actuators using fuzzy logic and Hammerstein-Wiener compensation, Mathematics 8 (11) (2020), https://doi.org/10.3390/math8112071.

[53] P.-Z. Li, D.-F. Zhang, J.-Y. Hu, B. Lennox, F. Arvin, Hysteresis modelling and feedforward control of piezoelectric actuator based on simplified interval type-2 fuzzy system, Sensors 20 (9) (2020), https://doi.org/10.3390/s20092587.

[54] J. Zhou, L. Dong, W. Yang, Hysteresis compensation for a piezoelectric actuator of active helicopter rotor using compound control, Micromachines 12 (11) (2021), https://doi.org/10.3390/mi12111298.

[55] R. Xiong, X. Liu, Z. Lai, Modeling of hysteresis in piezoelectric actuator based on segment similarity, Micromachines 6 (2015) 1805–1824, https://doi.org/10.3390/mi6111456.

[56] Y. Qin, H. Duan, Single-neuron adaptive hysteresis compensation of piezoelectric actuator based on Hebb learning rules, Micromachines 11 (2020) 84, https://doi.org/10.3390/mi11010084.

[57] M. Holčapek, L. Nguyen, T. Tichý, Polynomial alias higher degree fuzzy transform of complex-valued functions, in: Theme: Fuzzy Transforms and Fuzzy Systems, Fuzzy Sets Syst. 342 (2018) 1–31, https://doi.org/10.1016/j.fss.2017.06.011.

[58] P. Zitek, J. Fišer, T. Vyhlídal, IAE optimization of PID control loop with delay in pole assignment space, in: 13th IFAC Workshop on Time Delay Systems TDS 2016, IFAC-PapersOnLine 49 (10) (2016) 177–181, https://doi.org/10.1016/j.ifacol.2016.07.521.

[59] P.V. de Campos Souza, E. Lughofer, An advanced interpretable fuzzy neural network model based on uni-nullneuron constructed from n-uninorms, in: Fuzzy and Neurofuzzy Systems, Fuzzy Sets Syst. 426 (2022) 1–26, https://doi.org/10.1016/j.fss.2020.11.019.

[60] I.A. Martin, R.A. Irani, A generalized approach to anti-sway control for shipboard cranes, Mech. Syst. Signal Process. 148 (2021) 107168, https://doi.org/10.1016/j.ymssp.2020.107168.

[61] J. Phillips, E. Cripps, J.W. Lau, M. Hodkiewicz, Classifying machinery condition using oil samples and binary logistic regression, Mech. Syst. Signal Process. 60–61 (2015) 316–325, https://doi.org/10.1016/j.ymssp.2014.12.020.

[62] F. Jiang, L. Dong, Q. Dai, D.C. Nobes, Using wavelet packet denoising and ANFIS networks based on COSFLA optimization for electrical resistivity imaging inversion, in: Theme: Applications, Fuzzy Sets Syst. 337 (2018) 93–112, https://doi.org/10.1016/j.fss.2017.07.009.

[63] V. Ewald, R. Sridaran Venkat, A. Asokkumar, R. Benedictus, C. Boller, R.M. Groves, Perception modelling by invariant representation of deep learning for automated structural diagnostic in aircraft maintenance: a study case using DeepSHM, Mech. Syst. Signal Process. (2021) 108153, https://doi.org/10.1016/j.ymssp.2021.108153.

[64] J. Drgoňa, D. Picard, M. Kvasnica, L. Helsen, Approximate model predictive building control via machine learning, Appl. Energy 218 (2018) 199–216, https://doi.org/10.1016/j.apenergy.2018.02.156.

[65] B.M. Negash, A.D. Yaw, Artificial neural network based production forecasting for a hydrocarbon reservoir under water injection, Pet. Explor. Dev. 47 (2) (2020) 383–392, https://doi.org/10.1016/S1876-3804(20)60055-6.

[66] A. Movsessian, D. García Cava, D. Tcherniak, An artificial neural network methodology for damage detection: demonstration on an operating wind turbine blade, Mech. Syst. Signal Process. 159 (2021) 107766, https://doi.org/10.1016/j.ymssp.2021.107766.

[67] X. Zhang, L. Sun, Optimization of optical machine structure by backpropagation neural network based on particle swarm optimization and Bayesian regularization algorithms, Materials 14 (11) (2021), https://doi.org/10.3390/ma14112998.

[68] E. Sariev, G. Germano, Bayesian regularized artificial neural networks for the estimation of the probability of default, Quant. Finance 20 (2) (2020) 311–328, https://doi.org/10.1080/14697688.2019.1633014.

[69] B. Wyrwoł, Implementation of the FATI hierarchical fuzzy inference system using the immutability decomposition method, in: Neural Networks and Fuzzy Systems, Fuzzy Sets Syst. 381 (2020) 105–123, https://doi.org/10.1016/j.fss.2019.04.024.

[70] E.N. Sadjadi, Smooth compositions are candidates for robust fuzzy systems, in: Fuzzy and Neurofuzzy Systems, Fuzzy Sets Syst. 426 (2022) 66–93, https://doi.org/10.1016/j.fss.2021.04.006.

[71] W. He, R.M. Rodríguez, B. Dutta, L. Martínez, A type-1 OWA operator for extended comparative linguistic expressions with symbolic translation, Fuzzy Sets Syst. (2021), https://doi.org/10.1016/j.fss.2021.08.002.

[72] L. Zadeh, The concept of a linguistic variable and its application to approximate reasoning—I, Inf. Sci. 8 (3) (1975) 199–249, https://doi.org/10.1016/0020-0255(75)90036-5.

[73] M. Mizumoto, K. Tanaka, Some properties of fuzzy sets of type 2, Inf. Control 31 (4) (1976) 312–340, https://doi.org/10.1016/S0019-9958(76)80011-3.

[74] O. Castillo, L. Amador-Angulo, J.R. Castro, M. Garcia-Valdez, A comparative study of type-1 fuzzy logic systems, interval type-2 fuzzy logic systems and generalized type-2 fuzzy logic systems in control problems, Inf. Sci. 354 (2016) 257–274, https://doi.org/10.1016/j.ins.2016.03.026.

[75] X.-J. Wei, D.-Q. Zhang, S.-J. Huang, A variable selection method for a hierarchical interval type-2 TSK fuzzy inference system, in: Fuzzy and Neurofuzzy Models, Fuzzy Sets Syst. 438 (2022) 46–61, https://doi.org/10.1016/j.fss.2021.09.017.

[76] C. Suo, Y. Li, Z. Li, On n-polygonal interval-valued fuzzy sets, in: Fuzzy Intervals and Their Applications, Fuzzy Sets Syst. 417 (2021) 46–70, https://doi.org/10.1016/j.fss.2020.10.014.

[77] W. Wang, J.M. Mendel, Multiple attribute group decision making with linguistic variables and complete unknown weight information, Iran. J. Fuzzy Syst. 16 (4) (2019) 145–157, https://doi.org/10.22111/ijfs.2019.4788.

[78] J.C. Figueroa-García, H. Román-Flores, Y. Chalco-Cano, Type–reduction of interval type–2 fuzzy numbers via the Chebyshev inequality, in: Fuzzy Sets and Systems, 2021.

[79] N.N. Karnik, J.M. Mendel, Centroid of a type-2 fuzzy set, Inf. Sci. 132 (1) (2001) 195–220, https://doi.org/10.1016/S0020-0255(01)00069-X.

[80] R. Kurokawa, T. Sato, R. Vilanova, Y. Konishi, Discrete-time first-order plus dead-time model-reference trade-off PID control design, Appl. Sci. 9 (16) (2019), https://doi.org/10.3390/app9163220.

[81] I. Tejado, B.M. Vinagre, J.E. Traver, J. Prieto-Arranz, C. Nuevo-Gallardo, Back to basics: meaning of the parameters of fractional order PID controllers, Mathematics 7 (6) (2019), https://doi.org/10.3390/math7060530.

[82] J. Bae, K. Kim, S. Chu, J. Heo, S. Lim, S.W. Sung, Development of an antiwindup technique for a cascade control system, ACS Omega 5 (2020), https://doi.org/10.1021/acsomega.0c04927.

[83] L. Adamson, S. Fichera, B. Mokrani, J. Mottershead, Pole placement in uncertain dynamic systems by variance minimisation, Mech. Syst. Signal Process. 127 (2019) 290–305, https://doi.org/10.1016/j.ymssp.2019.03.007.

[84] H. Feng, C.-B. Yin, W. wen Weng, W. Ma, J. jing Zhou, W. hua Jia, Z. li Zhang, Robotic excavator trajectory control using an improved GA based PID controller, Mech. Syst. Signal Process. 105 (2018) 153–168, https://doi.org/10.1016/j.ymssp.2017.12.014.

[85] N.N. Son, C. Van Kien, H.P.H. Anh, Adaptive sliding mode control with hysteresis compensation-based neuroevolution for motion tracking of piezoelectric actuator, Appl. Soft Comput. 115 (2022) 108257, https://doi.org/10.1016/j.asoc.2021.108257.